

GF-1 and Landsat observed a 40-year wetland spatiotemporal variation and its coupled environmental factors in Yangtze River estuary

Nan Sun^a, Weining Zhu^{b,*}, Qian Cheng^c

^a Institute for Island and Coast Research, Ocean College, Zhejiang University, Zhoushan, China

^b Department of Marine Information Science, Ocean College, Zhejiang University, Zhoushan, China

^c School of Tourism and Urban-Rural Planning, Zhejiang Gongshang University, Hangzhou, China



ARTICLE INFO

Keywords:

Wetland
Yangtze river estuary
Remote sensing
Long-time series
Spatiotemporal variations
Driving factors

ABSTRACT

Wetlands are health indicators of aquatic ecosystems and also vulnerable to regional environmental and socio-economic changes. For exploring wetland spatiotemporal variations in estuarine and coastal regions of the Yangtze River, we extracted wetland information from 40-year time-series images of Landsat, GF-1, and other satellites, using the classification method of decision tree. Potential environmental and socio-economic factors which may drive wetland variations were analyzed. Results show that the wetland area in Yangtze River estuary has increased 663 km², but it was only contributed by the increasing of human-made wetlands (767 km²), which were mostly caused by economic growth and constructions of human-made hydro-projects in Yangtze Delta. In comparison, natural wetlands, such as tidal flats and marshes, have decreased 163 km². Land reclamation has changed these natural wetlands into reservoirs, aquaculture ponds and paddy fields. Wetlands in Shanghai and Qidong urban regions were mainly affected by human activities, while wetland variations in Chongming Island were mainly controlled by natural factors such as the upstream discharge, precipitation, diurnal variation of tidal level and long-term sea level rising. The general trend is that the natural wetland was transformed into the human-made wetland, and the human-made wetland was transformed into construction land.

1. Introduction

As the most productivity ecosystem of the globe, wetlands imply abundant biological diversity and vitality (Barbier et al., 2011). The value of global ecosystem services in 2011 was \$125 trillion/yr, of which 45% was contributed by wetlands and coasts (Costanza et al., 2014). Wetlands play a critical indicator of global climate change – they contain approximately 12% of the global carbon pool and contribute more than 10% of the annual global CH₄ emissions (Solomon, 2007), and hence affect greenhouse gas concentrations (Zedler and Kercher, 2005). Additionally, known as the kidney of the earth, wetlands bear irreplaceable functions for flood reduction, pollutant degradation, and environmental amenity (Keddy, 2010; Reddy and D'angelo, 1997). Because of a variety of natural and human influences, however, wetlands are now suffering from serious losses related to global warming, sea level rising, and other environmental factors and anthropogenic activities (An et al., 2007; Day et al., 2008). Many countries and organizations have made a lot of laws and actions to protect and restore wetlands. After GlobWetland projects launched by European Space Agency in cooperation with the Ramsar Secretariat in 2003, GW-II project aimed to develop a Global Wetland Observation System (G-

WOS) at all geographical scales using Sentinel-2 with 10–60 m spatial resolution (Jones et al., 2009). The U.S. EPA (Environmental Protection Agency) and FWS (Fish & Wildlife Service) published a comprehensive report on the status and changes of wetlands in the United States between 2004 and 2009 (Dahl, 2011). From 2009 to 2013, China's SFA (State Forestry Administration) carried out the second national wetland survey. This survey was based on CBERS (China Brazil Earth Resources Satellite, 20 m spatial resolution) remote sensing as well as the field measurements. It analyzed wetland distributions and variations in China, and its results show that China's wetland area is 536,026 km² (5.58% of the total land use) by the end of 2013. Compared to the result of the first national wetland survey, wetland area has reduced 33,963 km² in a rate up to 8.82% (SFA, 2014).

Wetlands in the middle and lower water basin of Yangtze River form not only the natural wetland landscape such as shallow rivers, lakes and swamps, but also human-made wetland landscapes such as wetland parks, reservoirs, and ponds. As one of the world's largest alluvial estuaries, the region of Yangtze River estuary and its delta, including a world-class eco-island, Chongming island, is now the most developed zone in east China (Huang et al., 2008). Due to the vulnerability of coastal wetland ecosystem, wetlands in Yangtze estuary was affected by

* Corresponding author.

E-mail address: zhuwn@zju.edu.cn (W. Zhu).

multi-factors such as irregular semi-diurnal tide in moderate intensity (Wang et al., 2007), a large amount of sediment and flux from the upper watershed of the Yangtze River (Zhang et al., 2006), and agricultural irrigating projects (Yang et al., 2005). Now the Yangtze estuarine wetland is suffering from degradation by sea-level rising (Kirwan and Megonigal, 2013) and rapid human reclamation over the past four decades (Chen et al., 2016). To stop the reduction and degradation of wetlands in Yangtze River estuarine and coastal regions, it is necessary to conduct accurate monitoring and mapping their long-time series variations, understand and find out the major environmental and socioeconomic factors that lead to these variations.

Using remote sensing to monitor and assess wetlands is a comprehensive analytical method (Davranche et al., 2010; Rebelo et al., 2009) – by which not only the spatial-temporal wetland variations, but also the changes of surrounding LULC (land use and land cover) can be observed at large scale. Among all current available satellites and sensors, the Landsat series, with medium spatial resolution 30 or 60 m, have been widely applied for LULC classifications since 1972, and their images are well known as the best long-term remote sensing data compared with other satellites, such as the MODIS (Wulder et al., 2015). By using Landsat images, one has obtained detailed distribution of global land cover and dynamics of surface-water (Yamazaki and Trigg, 2016). By using Landsat enhanced thematic mapper plus (ETM+) data, wetland mappings were also made for the entire China (Niu et al., 2009), changes of China's coastal wetlands from 1970s to 2007 (Zuo et al., 2013), as well as the wetland changes (1979–2009) in the Pearl River estuary in south China (Zhao et al., 2010). The main data of this study are also based on Landsat images, but we also used the multispectral data provided by GF-1 PMS (GaoFen) sensor. The series of GF satellites is a High-Definition Earth Observation System (HDEOS) developed by CAST (China Academy of Space Technology). The GF-1 is equipped with two 2 m resolution panchromatic/8 m resolution multispectral cameras and four 16 m WVF (wide field of view) multispectral sensors. Because of their high spatial resolution and short revisit period, GF images have been widely used in environmental protection, land resources survey, and other fields (Xingfa and Xudong, 2015).

Although there are previous studies on China's terrestrial, estuarine and coastal wetlands, the long-term wetland monitoring and environmental driving-force analysis for Yangtze River estuary has not been well investigated. Wetland changes in Shanghai from 2003 to 2013 were detected by using FORMOSAT and Landsat TM imagery (Tian et al., 2015), but these studies did not contain the north zone of Yangtze River Estuary in Jiangsu Province and also excluded paddy field as a wetland type. Geographic spatial modeling was applied to forecast the effects of sea-level rising at Chongming Dongtan Nature Reserve (Tian et al., 2010), but wetland changes influenced by human activities have not been well explored in this site. Some scholars found that the reduction of sediment discharge caused by upstream project will decrease the deposition of tidal flat (Yang et al., 2005). However, others found a rapid accrete in Jiuduansha wetland (Tian et al., 2015). Moreover, remote sensing classification methods are quite important for wetland mapping and monitoring (Civco et al., 2002), but different methods may lead to different results. For example, the support vector machine (SVM) and object-oriented methods have been respectively applied to detect wetland changes in Poyang Lake but their results demonstrate considerable inconsistency (Dronova et al., 2011; Han et al., 2015).

Responding to the abovementioned concerns, the objectives of this study are: (1) mapping the current wetland distributions in Yangtze River estuarine and coastal regions and monitoring their time-series variations from 1979 to 2016, and (2) exploring the environmental and socioeconomic factors, such as the precipitation, river discharge, and regional GDP, which may drive the observed wetland changes. In addition, we also compare and hence determine the best remote sensing estuarine wetland classification method from several popular supervised and unsupervised ones, such as the maximum likelihood, decision tree, object-oriented, support vector machine, and iterative self-

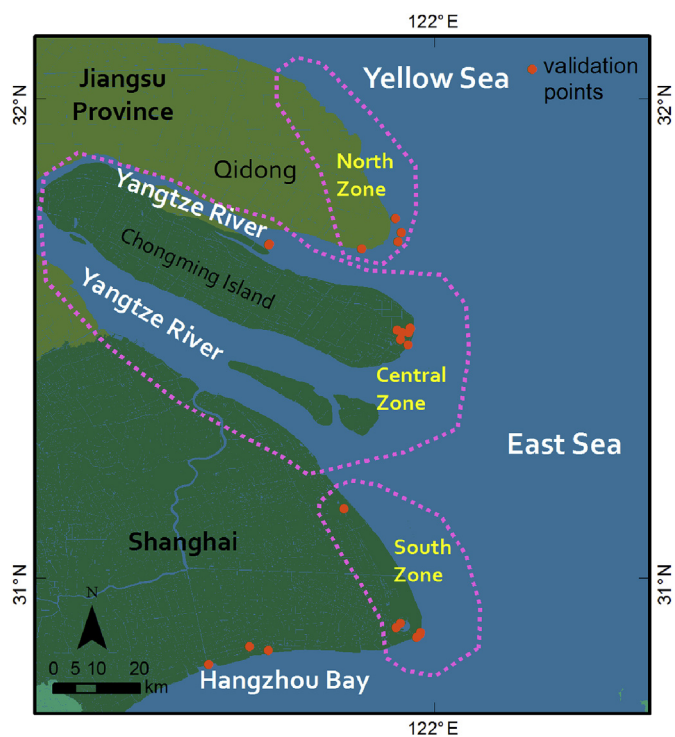


Fig. 1. Study site in Yangtze River estuary.

organizing data analysis. We expect this study will help to estuarine and coastal wetland mapping, monitoring, ecosystem restoration, biodiversity protection, as well as sustainable wetland management and development.

2. Data and methods

2.1. Study site

Yangtze River is the longest river in China (the 3rd longest in the world), with length 6300 km and watershed area 1.8 million km² (Chen et al., 2001). It forms the Yangtze Delta in its estuarine regions, including Shanghai municipality, the largest city in China, and parts of Jiangsu and Zhejiang Provinces, which are also China's most economically developed regions. Our study site consists of Shanghai and Qidong, a city of Jiangsu Province (Fig. 1). Due to the complicated riverine network system of Yangtze River (Liu et al., 2010), we divide the site into three sub-zones: (1) the north zone, including the coasts of Qidong and the small north branch of Yangtze River, (2) the south zone, including the coasts of Shanghai, and (3) the central zone, including the main channel of Yangtze River and three islands (Chongming, Changxing and Hengsha) in the mouth. There are many important wetland conservation areas in these zones, including two Ramsar-level wetland sites (Chongming Dongtan Nature Reserve and Shanghai Yangtze Estuarine Wetland Nature Reserve for Chinese Sturgeon), one national wetland site (Jiuduansha wetland) and two provincial reserves (Jinshan Three-island and Qidong Coastal Wetland).

Generally, the definition of coastal areas and the scope of wetland are quite flexible (Christian and Mazzilli, 2007). According to EPA and Ramsar Convention, coastal wetland may extend several miles from sea water (< 6 m depth) to inland area. To analyze the impact factors of coastal wetland and its adjacent areas, our study site was specifically focused on the regions between the land area 1 km apart from the coastal line at the average high tide and the sea water with depth less than 6 m at the average low tide. Moreover, our study area also covers a large area of cropland on the north and east of Chongming island – this area has been ignored in previous studies but they contain many paddy fields.

Table 1
Image data used in this study.

Date	Sensor	Scenes	Resolution (m)	Tidal level (CM)
10/24/1979	Landsat-2-MSS	2	60	150
07/07/1988	Landsat-5-TM	2	30	100
05/08/1995	Landsat-5-TM	2	30	20
06/06/2000	Landsat-5-TM	2	30	50
04/28/2009	Landsat-5-TM	2	30	80
07/20/2016	Landsat-8-OLI	2	30	72
08/03/2015	Landsat-8-OLI	2	30	90
08/02/2015	GF-1-PMS (1, 2)	13	8	110
08/02/2015	Google Earth (SPOT-7)	NA	1.5	NA

2.2. Images and processing

Data used in this study include 14 images from Landsat-MSS, TM, OLI (provided by USGS), 13 images from GF-1 PMS (provided by China Center for Resources Satellite Data and Application), and some images (SPOT-7) seen from the Google Earth (image copyright: Cnes/Astrium). Imageries acquisition time were selected from April to October, aiming

to minimize the land cover changes caused by different seasonal vegetation abundance and hydrological dynamics. All imageries are cloud-free. The detailed data information is listed in Table 1.

Images were processed by radiation calibration and geometrical correction, by using ENVI, a popular remote sensing image analysis software. Image DN (Digital Number) were converted to radiance L (unit: $\text{W}/(\text{m}^2 \times \text{sr} \times \mu\text{m})$) by the below formula,

$$L = \text{Gain} \times DN + \text{Offset} \quad (1)$$

where Gains and Offsets were obtained from the image metadata. NDVI (Normalized Difference Vegetation Index) and NDWI (Normalized Difference Water Index) were calculated through equations (2) and (3) for identifying vegetation and water (Gao, 1996; Rouse et al., 1974). Note that the atmospheric corrections were not made because it is known that atmospheric corrections do not improve accuracy for image classification (Lin et al., 2015; Song et al., 2001).

$$\text{NDVI} = \frac{\text{NIR} - \text{R}}{\text{NIR} + \text{R}} \quad (2)$$

$$\text{NDWI} = \frac{\text{G} - \text{NIR}}{\text{G} + \text{NIR}} \quad (3)$$

where NIR, R, and G refer to Near Infrared Red band, Red band and

Table 2
Wetland classes in Yangtze River Estuary.

Level I	Level II	Description	Class examples in images		
			Landsat-8	GF-1	SPOT-7
Natural Wetlands (NW)	Rivers and Lakes (NW1)	Permanent riverine and lacustrine wetland			
	Marsches (NW2)	Palustrine wetland with sparse vegetation			
	Tidal flat (NW3)	Non-vegetation foreshore, sand/mud shore			
	Shallow water (NW4)	Estuarine and coastal shallow water with depth < 6 m for mean low-tide line.			
Human-made wetlands (HW)	Reservoir (HW1)	Artificial water storage area			
	Aquaculture pond (HW2)	Human-made ponds for fish-farming			
	Paddy field (HW3)	Fields with planting rice, see Landsat-8 and GF-1 examples			
Non-wetland (LU)	Fallow land (LU1)	Fields with crops harvested, see SPOT-7 example			
	Build-up area (LU2)	Urban construction, impervious surface			
	Shrub and meadow (LU3)	Scrub with the height lower than 2m and grassland			

Green band, respectively.

2.3. Wetland classes

At national and regional scales, there are various classification schemes in accordance with Ramsar Convention (Ewart-Smith, 2006; Klemas et al., 1993). In our study site, wetland classes were identified and based on this Convention (Ramsar Convention Secretariat, 2013), China's National Standard of Wetland Classification (GB/T 24708-2009) (CSFA, 2010), visual interpretation of GF-1 and SPOT images, as well as our field observations. We visited the study site in November 24–25, 2016 (Fig. 1), and some typical wetlands were identified in the Dishui Lake, Dongtan Wetland Park, and many mariculture areas (Bey et al., 2016). As the results, wetlands in Yangtze River estuarine and coastal regions were classified to two major classes: natural wetlands (NW) and human-made wetlands (HW), and they can be further classified to four minor NW classes and three minor HW classes. The four NW classes are rivers and lakes (NW1), marshes (NW2), shoals (NW3), and estuarine and coastal shallow water (NW4). The three HW classes are reservoirs (HW1), paddy fields (HW2), and aquaculture fishponds (HW3). We also classified the non-wetland LULC into three classes: building lots (LU1), fallow land (LU2), and irrigated grassland (LU3). Note that the rice fields (HW2) are not permanent wetlands because they turn to be fallow land (LU2) when rice was harvested and fields became dry. Also, electronic nautical charts and navigation maps from arctiler.com were used to extract the water with depth < 6 m in 2009. According to spectral difference between deep water and shallow water, we can establish the relationship between water depth (y) and NDWI (x) by equation $y = 77.39x^2 - 16.63x + 5.01$ ($R^2 = 0.584$) to identify the area of shallow water in time-series images with accuracy $R^2 = 0.45$ and RMSE (root-mean-squared error) = 0.68 (Cho et al., 2008). The typical examples of the ten wetland and non-wetland classes visually interpreted from the Landsat, GF-1, and SPOT images and their descriptions are shown in Table 2.

2.4. Classification methods

Wetlands in GF-1 PMS images were classified by using e-Cognition 9.0, a well-known object-based image analysis software. The e-Cognition uses a GOBIAT (Geographic Object-Based Image Analysis Technique) method which contains two steps: (1) multi-solution segmentation based on region merging technology and (2) spectral difference segmentation analysis. We choose the scale parameter, the weight of shape criterion, and the weight of the compactness with values 20, 0.3 and 0.5, respectively. After several tests, all parameter settings met the best segmentation (Benz et al., 2004). The GF-1's results were further validated by the visual check of the Google Earth SPOT 7 image, which was acquired at the same day of the GF-1 image in Qidong but with higher spatial resolution (1.5 m). In addition, the image-derived wetland classes were also validated by in-situ observations in our fieldtrip in November 2016. We examined 30 selected check-points (Fig. 1), and classification accuracy is 96%, so we then take the GF-1's results as the ground truth and further used it to validate the classification results of Landsat images.

Five classification methods: maximum likelihood (ML), support vector machine (SVM), iterative self-organizing data analysis (isoData), decision tree (DT), and object-oriented (OO), were applied to the Landsat-OLI image acquired in 08/03/2015, just one day behind the GF-1's acquisition date. Compared to the GF-1's results, the accuracy evaluations of the Landsat-based classifications are listed in Table 3, which clearly shows that DT method is the best one with the highest accuracy and kappa coefficients. Therefore, we applied DT method to other Landsat time-series images and obtained the wetland classification results for Yangtze River estuary from 1979 to 2016. The latest classification results were also validated by our field observations. The typical wetlands in Nanhui, Chongming, and Qidong estuarine and

Table 3

Accuracy comparison of five classification methods using Landsat-8(08/03/2015).

Methods	Chongming east shores		Qidong coasts	
	Accuracy (%)	Kappa	Accuracy (%)	Kappa
Max. Likelihood	81.87	0.77	86.52	0.81
SVM	84.25	0.80	84.97	0.79
IsoData	64.41	0.52	65.64	0.51
Decision Tree	87.44	0.84	87.22	0.83
Object-oriented	85.28	0.81	86.01	0.82

coastal regions exactly matched our classification results in 2016 with the final overall accuracy 91% and kappa coefficient 0.89, respectively.

2.5. Environmental and socioeconomic data

The environmental and auxiliary data used in this study include (1) the monthly precipitation and air temperature over the Yangtze River estuarine regions (averaged for Qidong and Shanghai), obtained from CMDC (China Meteorological Data Service Center <http://data.cma.cn/en>), (2) the annual discharge and sediment runoff of Yangtze River and other rivers in the study area, according to Datong hydrologic station released by Yangtze Sediment Bulletin from Water Resources Commission (<http://www.cjw.gov.cn>), (3) electronic nautical charts and navigation maps from arctiler.com which were used to identify the water area with depth < 6 m, (4) tidal level table published by CNSS (China National Shipping Service), and (5) GDP and some agriculture data of Shanghai and Qidong (a city in Jiangsu Province), provided by statistical yearbooks or annual reports of the two cities.

3. Results and discussion

3.1. Classification results and accuracy assessment

Table 3 shows the accuracy assessment of five classification methods used in this study, in which the CART-based decision tree method gave the best accuracy 87% with Kappa coefficient 0.84 in Chongming east shore and also the best accuracy 87% with Kappa coefficient 0.83 in Qidong's coastal zones. The other three methods, ML, SVM, and OO, were with acceptable accuracies greater than 80% and Kappa coefficients greater than 0.8 (except that ML's Kappa = 0.77). The isoData method is with relatively lower accuracies 64% (Kappa 0.52) and 66% (Kappa 0.51) in Chongming east shore and Qidong's coastal zones, respectively. Fig. 2 shows the comparison of object-based classification between GF-1 and Landsat-8. GF-1 can identify smaller features, ditches and buildings scattered in farmlands due to its higher resolution. Although the OO method uses the spectral and spatial texture information in images, the classification accuracy of OO is slightly lower than that of DT for Landsat series.

Classification and Regression Tree (CART) uses data-training and machine-learning to develop classification rules to define each class. Traditional classification methods such as supervised classification only relies on the spectral information, but many studies have found that adding ancillary data into image classification as logical channels can increase classification accuracy (Jensen, 1986; Lawrence and Wright, 2001). Based on medium-resolution image data, CART-based DT method automatically combines the images with ancillary NDVI, topographical, and hydrological data, and then can improves the recognition of image textures, so it is superior to those traditional supervised and object-oriented classification methods (Baker et al., 2006; Lawrence and Wright, 2001; Zhao et al., 2014).

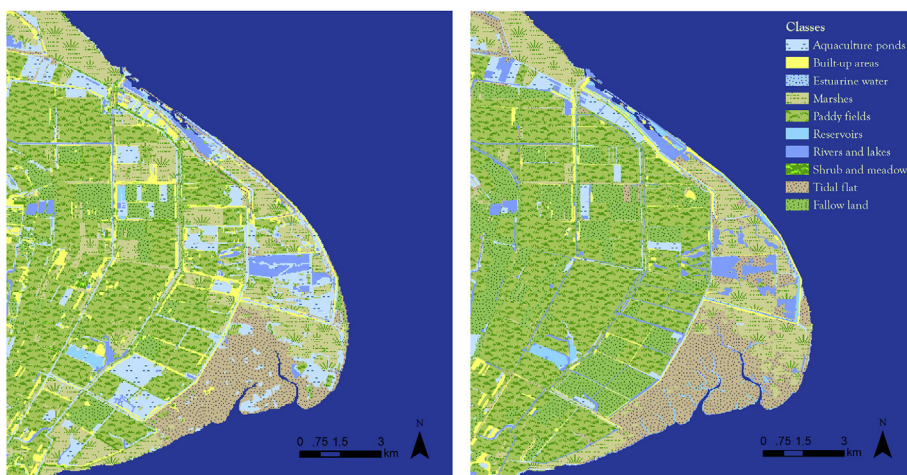


Fig. 2. Comparison of classification results: (a) using GF-1 and object-oriented method by e-Cognition, and (b) using Landsat-8 and object-oriented method by ENVI.

3.2. Current wetland distribution in Yangtze estuary

According to the results from GF-1 image acquired in 08/02/2015, Fig. 3 illustrates the respective proportions of different wetland classes in Yangtze River estuarine and coastal regions. The total wetland area is 4725 km², in which the natural wetland area accounts for 63.5% (3000 km²), the human-made wetland area accounts for 21.2% (1002 km²), and non-wetland accounts for 15.3% (723 km²). The 69% of the natural wetland is occupied by estuarine and coastal shallow water, and hence the terrestrial natural wetland only accounts for 21% (937 km²).

Different wetland classes distribute in different geographical regions. Chongming Dongtan and Jiuduansha island are covered with large tracts of intertidal marshes and mudflats caused by estuarine siltation. Among the human-made wetland, aquaculture ponds (149 km²) were found in the north coastal of Qidong. Many paddy fields and fallow lands locate in the northern and eastern regions of Chongming island. The land use for agriculture is 485 km² in central zone – the number is close to the area number (506 km²) published in

Chongming's yearbook of 2016, indicating that the classification accuracy is excellent. Note that the yearbook reports the total agriculture land in Chongming island, but some scattered cropland in the middle of the island was not included in our study area. Accompanying the rapid economic development after China's reform and opening to the outside world, a large number of building lots in Shanghai's coasts, such as in Nanhui District, Pudong airport, and other residential areas, have been constructed since late 1970's. Large-scale water resource conservation projects, such as the Qingcaosha reservoir and Deep-water Navigation Channel project in Jiuduansha (Li et al., 2016; Tong et al., 2010), have also increased about 109 km² human-made wetlands as wells as some non-wetland areas.

3.3. Wetland spatial-temporal variations

The Landsat-observed wetland distributions in from 1979 to 2016 in Yangtze estuarine and coastal regions are shown in Fig. 4, and we further analyzed the change of each wetland classes and its transfer model. Results show that the total wetland area has increased 663 km², in which human-made wetland has increased 767 km², construction land has increased 154 km², and natural wetland (shallow water excluded) has decreased 163 km² (Fig. 5). The natural wetland in 1979 was 1103 km², 868 km² more than human-made wetland, while human-made wetland reached 1002 km² in 2015, 66 km² more than natural wetland. Area changes of each NW, HW wetland classes and LULC are listed in Table 4. These figures demonstrate that natural wetland has been changed to farmland and other human-made wetland despite intensive sediment deposition in the estuary. Both sides of the Yangtze estuary are discovered with remarkable increases in build-up areas (214 km² in total).

From 1988 to 2015 in Yangtze estuary, coastal lands have gained of 872 km² and water gained of 75 km², which is consistent with the results of previous monitoring of global surface water dynamics from 1985 to 2015 (Donchyts et al., 2016). There is a general wetland variation that estuarine shallow water was transformed into mud flats and marshes, and then further changed to cropland, aquaculture ponds and reservoirs. During the same period, parts of natural and human-made wetlands were transformed to build-up lots with areas 99 km² and 86 km², respectively. In addition, results also show that the conversions between paddy field and fallow land occurred following the seasonal changes (Huang et al., 2010; Liu et al., 2003).

Fig. 6(a) shows the wetland variations at different estuarine and coastal zones over the past 40 years. The wetland in the north zone has slightly increased 77 km², in which human-made wetland has increased 136 km², but natural wetland has lost 59 km². The emerged HWs are mainly reservoir (HW1) and mariculture ponds (HW2). The wetland in

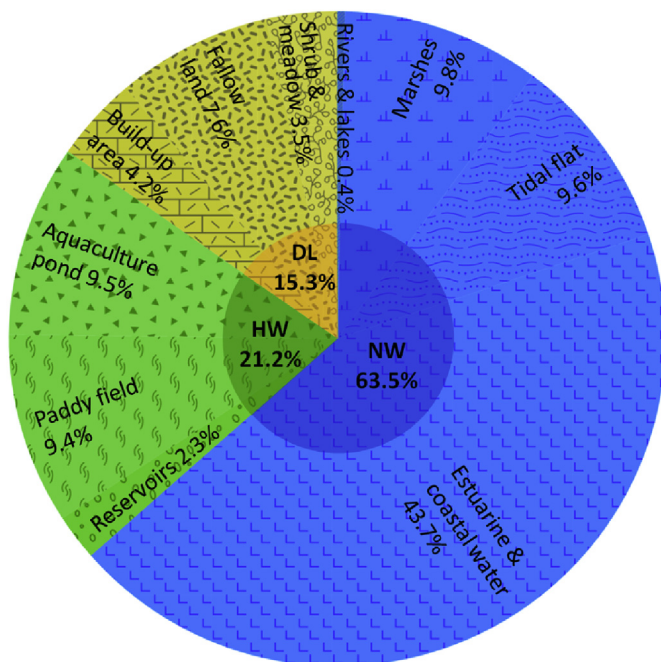


Fig. 3. Natural wetland, human-made wetland, and dryland proportions estimated from the GF-1 image acquired in 2015.

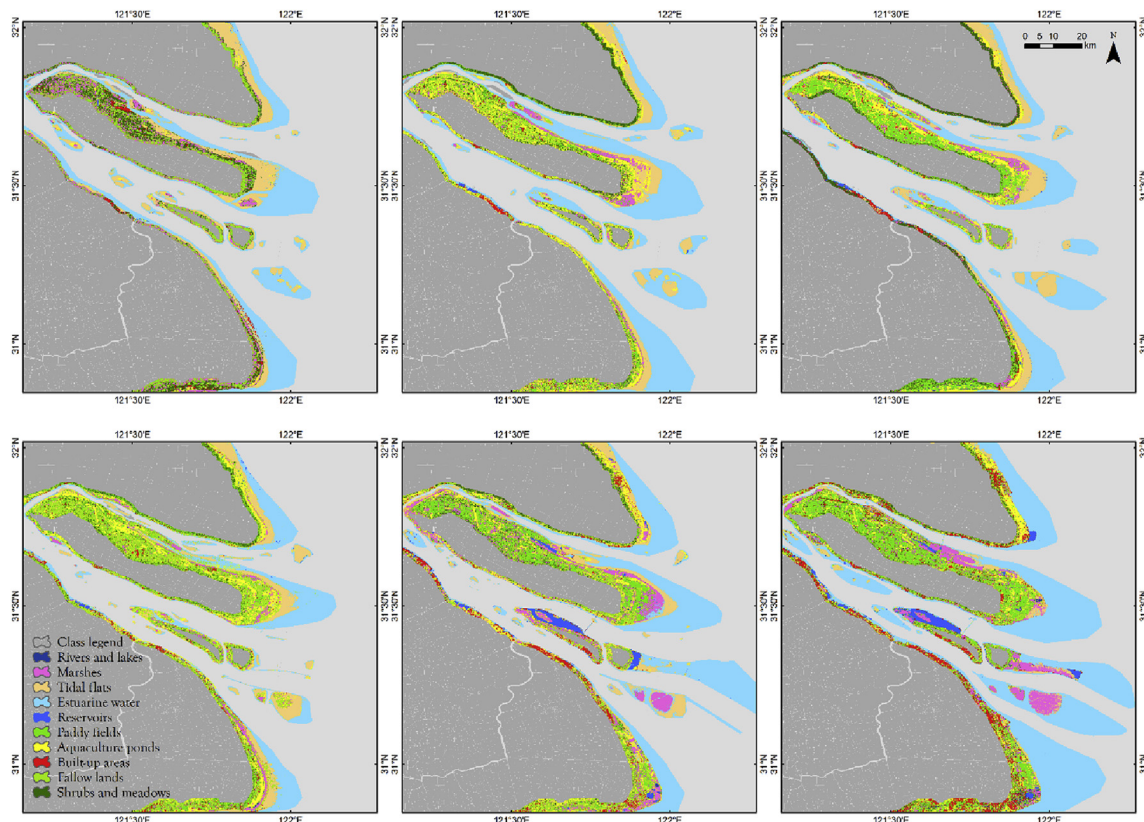


Fig. 4. Wetland distribution and variations in Yangtze River estuary over 40 years. (a) 1979, (b) 1988, (c) 1995, (d) 2000, (e) 2009, (f) 2016.

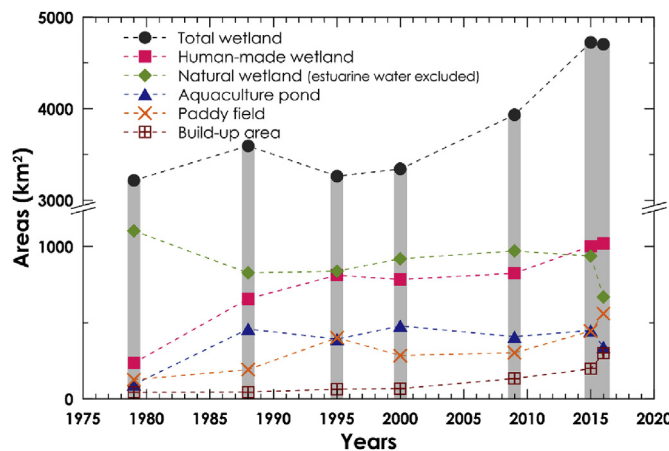


Fig. 5. 40-year area changes of different wetland classes.

the south zone has not demonstrated obvious change during 1979–2009, but shown a significant increasing (367 km^2) after year 2009. Large areas of new mariculture ponds (HW2) were observed, which were mainly transformed from the tidal flats (NW3). Within the central zone, total wetland area firstly has gained hundreds of square kilometers since 1979 but returned to its initial amount in late 1990's, within the area of $1500 \pm 200 \text{ km}^2$, but after 2000, the wetland area in this zone got a significant increasing (1034 km^2).

For each study year, only one image was used to estimate the wetland area, so the estimated result may not be exactly equal to the mean wetland area in that year, since there are many uncertainties related to that image, for example, uncertainties caused by flood, typhoon, and short temporal human activities such as the irrigations. Therefore, to reduce the uncertainty and improve estimation accuracy, the images used for wetland classifications should be as many as possible in future studies.

3.4. Driving factor analysis in three zones

The sediment deposition and water discharge of the Yangtze River and precipitation in its estuarine regions as well as economic data (GDP) collected from 1979 to 2016 were analyzed for the driving factors of wetland variations, as shown in Fig. 6(b)-(d) and Fig 7(c). Results indicate that different zones were impacted by different factors.

3.4.1. Socio-economic driving factor analysis in north and south zones

Qidong coastal wetland in the north zone and Nanhui Dongtan wetland in the south zone were both more affected by anthropogenic activities. The coastal mudflat area in Qidong was 342 km^2 in 1979, but only 163 km^2 in 2015, making annual loss of 4.9%. Reclamation of tidal flats has been greatly enhanced in recent years since these flats are important reserved land resources, which can be utilized in agriculture and industry in response to the rapid urbanization of Yangtze Delta (Chen et al., 2016). Along with the rapid population boom, the urbanization area in Shanghai is predicted to be 1474 km^2 by 2020 with an average annual rate 3% (Han et al., 2009). Mudflats have been converted into human-made wetland and coastal water conservancy projects. Reservoirs and aquaculture ponds have experienced a gain of 135 km^2 while the built-up areas have experienced a gain of 62 km^2 . At the same time, the total area of human-made wetland in Nanhui Dongtan has increased 170 km^2 and build-up area has added 77 km^2 over the past 40 years. The image results clearly show the expanding trend of waterlines and its corresponding area changing in Nanhui (Fig. 8(c) and 8(d)). Correspondingly, the GDPs of Qidong and Shanghai have shown a rapid increasing since the last century 80's (Fig. 7(c)). The same trend is also coupled between GDP and the total areas of reservoirs and aquaculture ponds plus build-up lots, the major human-made wetlands, but the opposite trend were seen between GDP and the area of tidal flat, which is a typical natural wetland (Fig. 7(a) and (b)).

Table 4Wetland area variations in the Yangtze River estuary from 1979 to 2016 (unit: km²).

Area(km ²)	1979	1988	1995	2000	2009	2015	2016	Variations
NW1	3.1	3.1	6.3	3.7	7.7	18.5	22.5	19.4
NW2	359.6	221.0	232.5	197.8	449.4	461.5	397.3	37.7
NW3	740.3	602.1	599.1	718.0	513.4	456.6	247.7	-492.7
NW4	1213.8	1580.2	1198.3	854.3	1411.4	2062.9	2282.3	1068.5
HW1	15.5	5.9	18.3	18.4	113.8	107.5	121.1	105.7
HW2	94.0	458.6	392.0	479.2	408.1	449.4	340.8	246.8
HW3	125.9	192.0	400.9	284.9	302.5	445.4	559.1	433.2
LU1	308.2	260.7	74.4	573.7	429.7	360.9	290.3	-17.9
LU2	43.3	44.8	63.1	67.2	133.8	197.6	300.5	257.1
LU3	312.2	224.5	277.5	142.4	163.2	164.5	142.0	-170.2
NW	1103.0	826.2	837.9	919.5	970.5	936.6	667.5	-435.6
HW	235.4	656.4	811.1	782.6	824.4	1002.3	1021.1	785.6
LU	663.8	530.0	415.1	783.4	726.7	723.0	732.8	69.1
Total	3216.1	3592.8	3262.4	3339.7	3933.0	4724.8	4703.7	1487.6

3.4.2. Environmental driving factor analysis in central zone

In Yangtze River estuary, the growth of natural wetland was found mostly in the central zone, which includes the east shore of Chongming Island and part of Jiuduansha. Wetland variations in this zone were more controlled by environmental factors such as stream flow and precipitation. During the flood season (June to September) when the Yangtze River is suffering from large monsoonal runoff and rainfall in its estuarine regions, the natural wetland in central zone usually

experiences significant shrinking. In 2000, for example, the precipitation and discharge of the Yangtze River were higher than those in neighboring years, resulting in a reduction of wetland in the central zone. The similar case was also reported in Poyang Lake (the largest freshwater lake attached to the Yangtze River) wetland during the wet season (Feng et al., 2016). Large amount of water discharge and sediments were brought to the estuary, while tidal flats and marshes were washed into the sea by plenty of water for a long time. At the same

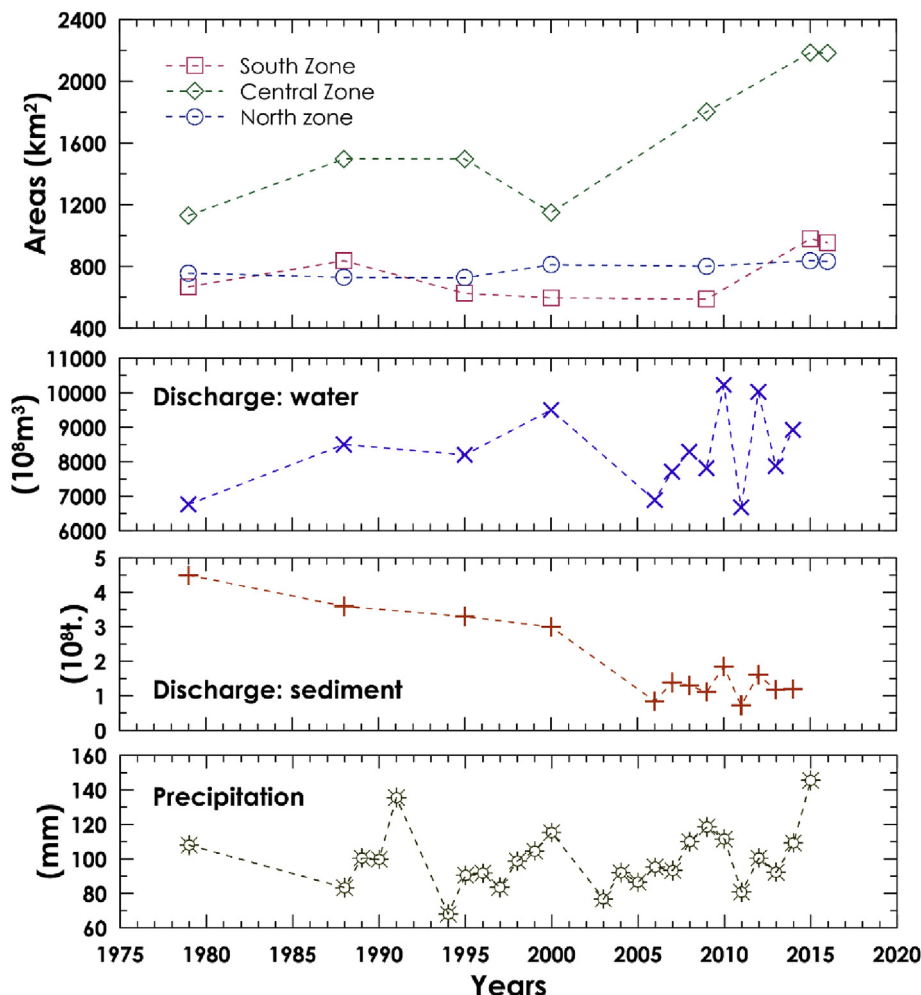


Fig. 6. Wetland area changes in different zones coupled with environmental factors in Yangtze River estuarine region (a) the discharge of water, (b) the discharge of sediments, and (c) the precipitation of the region.

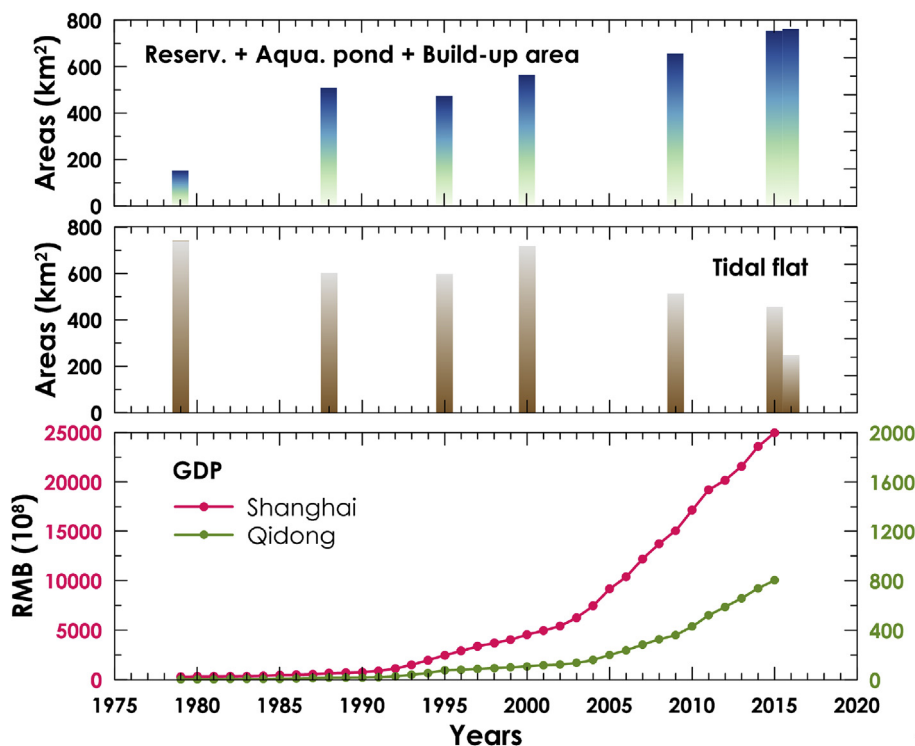


Fig. 7. 40-year changes of tidal flats and RAB wetlands versus GDP growth of Shanghai and Qidong.

time, large area of marshes was submerged by sea water.

The CDNR (Chongming Dongtan Nature Reserve) is extremely vulnerable and sensitive to accelerated sea-level rising caused by global warming in recent years (Wang et al., 2007; Zhao et al., 2008). Some studies indicate that about 40% of the terrestrial area in Chongming Dongtan will be inundated by the year 2100 because of a predicted 0.88 m sea-level rising (Tian et al., 2010). As a tidal wetland site, intertidal wetlands were also controlled by irregular semi-diurnal tides. Compared to previous years, natural wetland in CDNR in 2016 experienced a loss of mudflat for 208 km², corresponding to the higher tide level in 2015, which is higher than that in 2016 depending on Table 1 (20–30 cm higher at the image acquisition time).

The sediment deposition of Yangtze River is also an important environmental factor which can change wetland areas via changing its estuarine morphological features and tidal flats. The change of waterlines and corresponding areas from 1979 to 2015 in Chongming Dongtan were presented in Fig. 8(a) and (b). The main tendency of average waterline is extending outward, but also appeared that islands formed by tidal flat were submerged by seawater during 1979 and 1988. In order to detect the depositions at different orientations, we divide Chongming Dongtan into seven sections (S1-S7). S1-S2 locate in the river channel between Qidong and Chongming Island, and the S6-S7 locate between Changxing Island and Chongming Island, see Fig. 8(b). Through the past 40 years, the deposition area in Chongming Dongtan reaches 175.42 km², in which 68.2% is at S3-S5. It is found that sections S3-S5 are in the fastest growth rate, but the total rate is declining rapidly. The mean annual growth rate of the seven sections was 1.49 km² from 1979 to 1988, but it was only 0.28 km² from 2009 to 2015. It is also found that the growth rate of Dongtan wetland was significantly slowed down since 2000 – the previous studies indicate that it may be related to the deposition changing made by some hydraulic engineering projects in upper Yangtze River, such as the TGD (Three Gorges Dam) (Feng et al., 2016; Yang et al., 2007). After year 2002 as the Dam was firstly finished, there is a significant downward trend of sediment discharge of the Yangtze River (Fig. 6(c)).

Some large climate events related to the Yangtze River Delta may

also affect natural wetland variations potentially. It is found that long-term changes of stream flow and precipitation of lower Yangtze River may be coupled with ENSO and other large-scale atmospheric circulations (Zhang et al., 2007, 2008). Not only the anthropogenic sediment trapping in upstream reservoirs is the dominant factor for decrease in sediment, but also the fluvial suspended sediment loads can be reduced by climate events such as tropical cyclones (Darby et al., 2016). Other environmental factors such as the intensified soil erosion may cause more terrestrial detritus into estuarine and coastal waters and hence increase wetland area for shallow water (Cui et al., 2013).

4. Conclusion

The maximum likelihood, SVM, decision tree, and object-oriented methods are all good for wetland remote sensing classification in estuarine and coastal regions, and the decision tree is recommended as the best one, while isoData method is not good for wetland classification because of its relatively low accuracy. GF-1 PMS images with high spatial resolution are good for object-oriented wetland classifications, which can identify smaller surface features, using the spatial texture and spectral information. CART-based decision tree automatically combines multispectral data and ancillary data, and then can greatly improve classification accuracy.

In 2015, wetland area in Yangtze River estuarine and coastal regions was 4725 km², in which the natural wetland area was 3000 km² and human-made wetland area was 1002 km². Most of wetlands are estuarine and coastal shallow water (2,063 km²), marshes (461 km²), tidal flats (457 km²), aquaculture ponds (449 km²), paddy fields (445 km²), and reservoirs (107 km²). From 1979 to 2016, the total wetland area has increased 663 km² – the growth of human-made wetlands positively contributed to 767 km² due to the development and constructions of large reservoirs, aquaculture ponds, and ports. The natural wetlands area shrunk to 920 km² in 2000. After that, the natural wetland coverage kept relatively stable due to the enhancement of wetland protection and management. There was also a significant increase of built-up area due to rapidly economic development. The

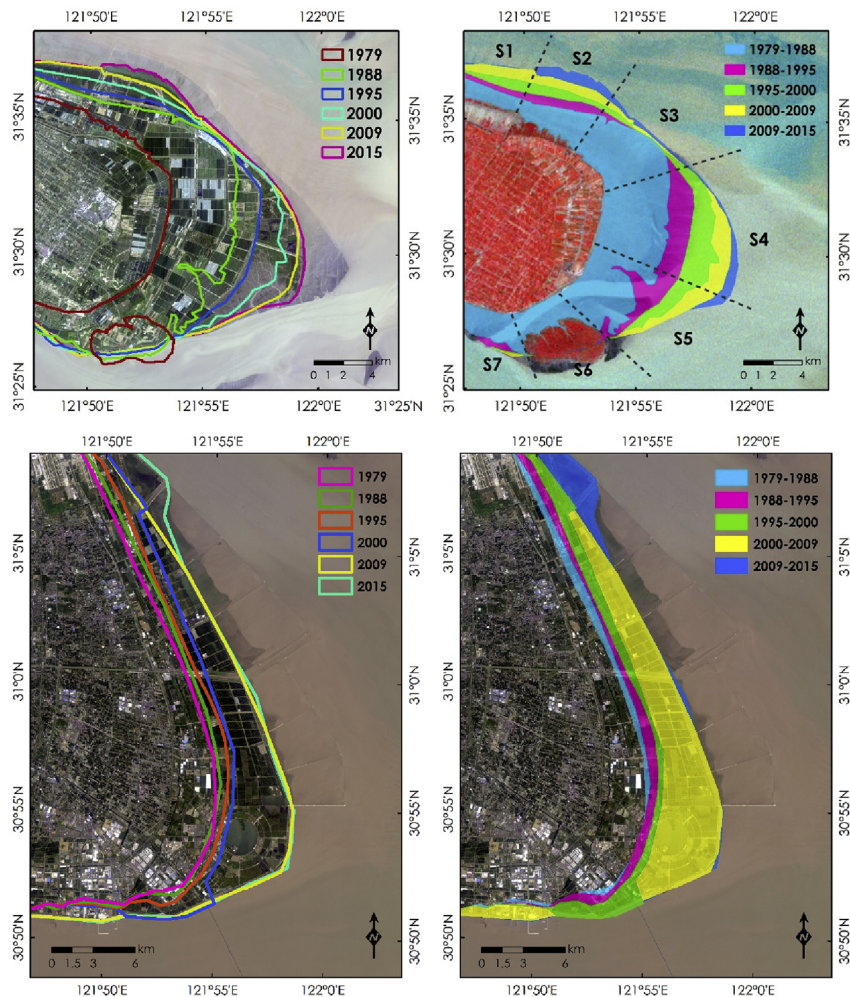


Fig. 8. Changes of average waterline and wetland areas of the east shores of Chongming ((a) and (b)) and Nanhui ((c) and (d)).

general trend in Yangtze River estuary is that natural wetland was transformed into human-made wetland, and human-made wetland was transformed into construction land.

Wetland changes in north, south, and central zones of Yangtze River estuarine and coastal regions demonstrated distinctive characteristics and were driven by different factors. The emerged human-made wetlands were mainly paddy fields in the south, but in the north they were reservoirs and mariculture zones. The increase of human-made wetland coincided with the economic development in Qidong and Nanhui Dongtan coasts, where wetland has been transformed from tidal flat and shallow water to human-made wetland and building-up land. The increased natural wetland were mainly marshes and mudflats in the Chongming Island, Changxing Island and Jiuduansha Island. The average waterline of Chongming Dongtan wetland has expended since 1979, making a deposition area 175 km². At the same time, the growth rate of natural wetland suffered to a rapid decline caused by sea-level rising and sediment supply reduction. The large-scale climate changes that change river flow and precipitation also influence wetland variation in the estuarine regions. All results show that a series of environmental factors determined the wetland area of central branch in Yangtze River estuary. Some minor uncertainties may remain in results due to the relatively low temporal resolution of the used satellite images, and we expect these uncertainties can be reduced in future by using more images with higher temporal resolution, especially for monthly average or annual average value of land classification and water depth estimation.

Acknowledgement

This research is supported by the National Natural Science Foundation of China (No. 41471346 and 41271417) and the High Resolution Earth Observation Systems of National Science and Technology Major Projects (No. 05-Y30B02-9001-13/15-4) of the Ministry of Environmental Protection of China (the sub-project ‘remote sensing of wetland ecosystem changes and analysis of its hydrological driving effects in Yangtze River estuary’).

Appendix A. Supplementary data

Supplementary data related to this article can be found at <http://dx.doi.org/10.1016/j.ecss.2018.03.022>.

References

- An, S., Li, H., Guan, B., Zhou, C., Wang, Z., Deng, Z., Zhi, Y., Liu, Y., Xu, C., Fang, S., 2007. China's natural wetlands: past problems, current status, and future challenges. *AMBIO A J. Hum. Environ.* 36, 335–342.
- Baker, C., Lawrence, R., Montagne, C., Patten, D., 2006. Mapping wetlands and riparian areas using Landsat ETM+ imagery and decision-tree-based models. *Wetlands* 26, 465–474.
- Barbier, E.B., Hacker, S.D., Kennedy, C., Koch, E.W., Stier, A.C., Silliman, B.R., 2011. The value of estuarine and coastal ecosystem services. *Ecol. Monogr.* 81, 169–193.
- Benz, U.C., Hofmann, P., Willhauck, G., Lingenfelder, I., Heynen, M., 2004. Multi-resolution, object-oriented fuzzy analysis of remote sensing data for GIS-ready information. *ISPRS J. Photogrammetry Remote Sens.* 58, 239–258.
- Bey, A., Sánchez-Paus Díaz, A., Maniatis, D., Marchi, G., Mollicone, D., Ricci, S., Bastin, J.-F., Moore, R., Federici, S., Rezende, M., 2016. Collect earth: land use and land

- cover assessment through augmented visual interpretation. *Rem. Sens.* 8, 807.
- CSFA, 2010. Chinese State Forestry Administration (2010) Wetland Classification. Standards press of China, Beijing. <http://e-file.shidi.org/exposed/dload/?fid=746>.
- Chen, Y., Dong, J., Xiao, X., Zhang, M., Tian, B., Zhou, Y., Li, B., Ma, Z., 2016. Land claim and loss of tidal flats in the Yangtze Estuary. *Sci. Rep.* 6.
- Chen, Z., Yu, L., Gupta, A., 2001. The Yangtze River: an introduction. *Geomorphology* 41, 73–75. [https://doi.org/10.1016/S0169-555X\(01\)00105-2](https://doi.org/10.1016/S0169-555X(01)00105-2).
- Cho, H.J., Kirui, P., Natarajan, H., 2008. Test of multi-spectral vegetation index for floating and canopy-forming submerged vegetation. *Int. J. Environ. Res. Publ. Health* 5 (5), 477–483.
- Christian, R.R., Mazzilli, S., 2007. Defining the coast and sentinel ecosystems for coastal observations of global change. *Hydrobiologia* 577, 55–70.
- Civco, D.L., Hurd, J.D., Wilson, E.H., Song, M., Zhang, Z., 2002. A comparison of land use and land cover change detection methods. In: ASPRS-ACSM Annual Conference.
- Costanza, R., de Groot, R., Sutton, P., van der Ploeg, S., Anderson, S.J., Kubiszewski, I., Farber, S., Turner, R.K., 2014. Changes in the global value of ecosystem services. *Global Environ. Change* 26, 152–158.
- Cui, L., Gao, C., Zhao, X., Ma, Q., Zhang, M., Li, W., Song, H., Wang, Y., Li, S., Zhang, Y., 2013. Dynamics of the lakes in the middle and lower reaches of the Yangtze River basin, China, since late nineteenth century. *Environ. Monit. Assess.* 185, 4005–4018.
- Dahl, T.E., 2011. Status and Trends of Wetlands in the Conterminous United States 2004 to 2009. US Department of the Interior, US Fish and Wildlife Service, Fisheries and Habitat Conservation.
- Darby, S.E., Hackney, C.R., Leyland, J., Kummu, M., Lauri, H., Parsons, D.R., Best, J.L., Nicholas, A.P., Aalto, R., 2016. Fluvial sediment supply to a mega-delta reduced by shifting tropical-cyclone activity. *Nature* 539, 276–279.
- Davranche, A., Lefebvre, G., Poulin, B., 2010. Wetland monitoring using classification trees and SPOT-5 seasonal time series. *Remote Sens. Environ.* 114, 552–562.
- Day, J.W., Christian, R.R., Boesch, D.M., Yáñez-Arancibia, A., Morris, J., Twilley, R.R., Naylor, L., Schaffner, L., 2008. Consequences of climate change on the ecogeomorphology of coastal wetlands. *Estuar. Coast* 31, 477–491.
- Donchyts, G., Baart, F., Winsemius, H., Gorelick, N., Kwadijk, J., van de Giesen, N., 2016. Earth's surface water change over the past 30 years. *Nat. Clim. Change* 6, 810–813.
- Dronova, I., Gong, P., Wang, L., 2011. Object-based analysis and change detection of major wetland cover types and their classification uncertainty during the low water period at Poyang Lake, China. *Rem. Sens. Environ.* 115, 3220–3236.
- Ewart-Smith, J.L., 2006. National Wetland Inventory: Development of a Wetland Classification System for South Africa. Water Research Commission.
- Feng, L., Han, X., Hu, C., Chen, X., 2016. Four decades of wetland changes of the largest freshwater lake in China: possible linkage to the Three Gorges Dam? *Rem. Sens. Environ.* 176, 43–55.
- Gao, B.-C., 1996. NDWI—a normalized difference water index for remote sensing of vegetation liquid water from space. *Remote Sens. Environ.* 58, 257–266.
- Han, J., Hayashi, Y., Cao, X., Imura, H., 2009. Application of an integrated system dynamics and cellular automata model for urban growth assessment: a case study of Shanghai, China. *Landsc. Urban Plann.* 91, 133–141.
- Han, X., Chen, X., Feng, L., 2015. Four decades of winter wetland changes in Poyang Lake based on Landsat observations between 1973 and 2013. *Rem. Sens. Environ.* 156, 426–437.
- Huang, B., Ouyang, Z., Zheng, H., Zhang, H., Wang, X., 2008. Construction of an eco-island: a case study of Chongming Island, China. *Ocean Coast Manag.* 51, 575–588.
- Huang, Y., Sun, W., Zhang, W., Yu, Y., Su, Y., Song, C., 2010. Marshland conversion to cropland in northeast China from 1950 to 2000 reduced the greenhouse effect. *Global Change Biol.* 16, 680–695.
- Jensen, John R., 1986. Introductory digital image processing: a remote sensing perspective[J]. *Geocarto Int.* xv (1) 382–382.
- Jones, K., Lanthier, Y., van der Voet, P., van Valkengoed, E., Taylor, D., Fernández-Prieto, D., 2009. Monitoring and assessment of wetlands using Earth Observation: the GlobWetland project. *J. Environ. Manag.* 90, 2154–2169.
- Keddy, P.A., 2010. Wetland Ecology: Principles and Conservation. Cambridge University Press.
- Kirwan, M.L., Megonigal, J.P., 2013. Tidal wetland stability in the face of human impacts and sea-level rise. *Nature* 504, 53–60.
- Klemas, V.V., Dobson, J.E., Ferguson, R.L., Haddad, K.D., 1993. A coastal land cover classification system for the NOAA Coastwatch Change Analysis Project. *J. Coast Res.* 862–872.
- Lawrence, R.L., Wright, A., 2001. Rule-based classification systems using classification and regression tree (CART) analysis. *Photogramm. Eng. Rem. Sens.* 67, 1137–1142.
- Li, X., Liu, J.P., Tian, B., 2016. Evolution of the Jiuduansha wetland and the impact of navigation works in the Yangtze Estuary, China. *Geomorphology* 253, 328–339.
- Lin, C., Wu, C.-C., Tsogt, K., Ouyang, Y.-C., Chang, C.-I., 2015. Effects of atmospheric correction and pansharpening on LULC classification accuracy using WorldView-2 imagery. *Inf. Process. Agric.* 2, 25–36.
- Liu, H., He, Q., Wang, Z., Weltje, G.J., Zhang, J., 2010. Dynamics and spatial variability of near-bottom sediment exchange in the Yangtze Estuary, China. *Estuar. Coast Shelf Sci.* 86, 322–330.
- Liu, J., Liu, M., Zhuang, D., Zhang, Z., Deng, X., 2003. Study on spatial pattern of land-use change in China during 1995–2000. *Sci. China Earth Sci.* 46, 373–384.
- Niu, Z., Gong, P., Cheng, X., Guo, J., Wang, L., Huang, H., Shen, S., Wu, Y., Wang, X., Wang, X., 2009. Geographical characteristics of China's wetlands derived from remotely sensed data. *Sci. China Earth Sci.* 52, 723–738.
- Ramsar Convention Secretariat, 2013. The Ramsar Convention Manual, sixth ed. The Secretariat of the Convention on Wetlands, Gland, Switzerland Accessed December 8.
- Rebelo, L.-M., Finlayson, C.M., Nagabhatla, N., 2009. Remote sensing and GIS for wetland inventory, mapping and change analysis. *J. Environ. Manag.* 90, 2144–2153.
- Reddy, K., D'angelo, E., 1997. Biogeochemical indicators to evaluate pollutant removal efficiency in constructed wetlands. *Water Sci. Technol.* 35, 1–10.
- Rouse Jr., J.W., Haas, R., Schell, J., Deering, D., 1974. Monitoring Vegetation Systems in the Great Plains with ERTS. NASA special publication 351, pp. 309. https://ntrs.nasa.gov/search.jsp?R=1_9740022614.
- SFA, 2014. The result of second national wetland survey. *Wetland Science & Management* 01, 65.
- Solomon, S., 2007. Climate Change 2007—the Physical Science Basis: Working Group I Contribution to the Fourth Assessment Report of the IPCC. Cambridge University Press. https://www.ipcc.ch/publications_and_data/publications_ipcc_fourth_assessment_report_wg1_report_the_physical_science_basis.htm.
- Song, C., Woodcock, C.E., Seto, K.C., Lenney, M.P., Macomber, S.A., 2001. Classification and change detection using Landsat TM data: when and how to correct atmospheric effects? *Rem. Sens. Environ.* 75, 230–244.
- Tian, B., Zhang, L., Wang, X., Zhou, Y., Zhang, W., 2010. Forecasting the effects of sea-level rise at chongming dongtan nature reserve in the Yangtze delta, Shanghai, China. *Ecol. Eng.* 36, 1383–1388.
- Tian, B., Zhou, Y.-X., Thom, R.M., Diefenderfer, H.L., Yuan, Q., 2015. Detecting wetland changes in Shanghai, China using FORMOSAT and Landsat TM imagery. *J. Hydrol.* 529, 1–10.
- Tong, C., Zheng, J., Zhang, C., Guilbaud, C., 2010. Salinity response to the runoff from Yangtze River basin at Qingcaoha reservoir area in Yangtze estuary. In: ASME 2010 29th International Conference on Ocean, Offshore and Arctic Engineering. American Society of Mechanical Engineers, pp. 247–255.
- Wang, Z., Li, L., Chen, D., Xu, K., Wei, T., Gao, J., Zhao, Y., Chen, Z., Masabate, W., 2007. Plume front and suspended sediment dispersal off the Yangtze (Changjiang) River mouth, China during non-flood season. *Estuarine. Coastal and Shelf Science* 71, 60–67.
- Wulder, M.A., White, J.C., Loveland, T.R., Woodcock, C.E., Belward, A.S., Cohen, W.B., Fosnight, E.A., Shaw, J., Masek, J.G., Roy, D.P., 2015. The global Landsat archive: status, consolidation, and direction. *Rem. Sens. Environ.* 185, 271–283.
- Xingfa, G., Xudong, T., 2015. Overview of China earth observation satellite programs [space agencies]. *IEEE Geosci. Rem. Sens. Mag.* 3, 113–129.
- Yamazaki, D., Trigg, M.A., 2016. Hydrology: the dynamics of Earth's surface water. *Nature* 540, 348–349.
- Yang, S., Zhang, J., Xu, X., 2007. Influence of the three Gorges Dam on downstream delivery of sediment and its environmental implications, Yangtze River. *Geophys. Res. Lett.* 34.
- Yang, S., Zhang, J., Zhu, J., Smith, J., Dai, S., Gao, A., Li, P., 2005. Impact of dams on Yangtze River sediment supply to the sea and delta intertidal wetland response. *J. Geophys. Res. Earth Surf.* 110.
- Zedler, J.B., Kercher, S., 2005. Wetland resources: status, trends, ecosystem services, and restorability. *Annu. Rev. Environ. Resour.* 30, 39–74.
- Zhang, Q., Xu, C.-y., Becker, S., Jiang, T., 2006. Sediment and runoff changes in the Yangtze River basin during past 50 years. *J. Hydrol.* 331, 511–523.
- Zhang, Q., Xu, C.-y., Jiang, T., Wu, Y., 2007. Possible influence of ENSO on annual maximum streamflow of the Yangtze River, China. *J. Hydrol.* 333, 265–274.
- Zhang, Q., Xu, C.-Y., Zhang, Z., Chen, Y.D., Liu, C.-L., Lin, H., 2008. Spatial and temporal variability of precipitation maxima during 1960–2005 in the Yangtze River basin and possible association with large-scale circulation. *J. Hydrol.* 353, 215–227.
- Zhao, B., Guo, H., Yan, Y., Wang, Q., Li, B., 2008. A simple waterline approach for tides using multi-temporal satellite images: a case study in the Yangtze Delta. *Estuarine. Coastal and Shelf Science* 77, 134–142.
- Zhao, H., Cui, B., Zhang, H., Fan, X., Zhang, Z., Lei, X., 2010. A landscape approach for wetland change detection (1979–2009) in the Pearl River Estuary. *Procedia Environ. Sci.* 2, 1265–1278.
- Zhao, S., Liu, Y., Jiang, J., Cheng, W., Zhou, M., Li, M., Ruan, R., 2014. Extraction of mangrove in Hainan Dongzhai Harbor based on CART decision tree. In: *Geoinformatics (GeoInformatics)*, 2014 22nd International Conference on. IEEE, pp. 1–6.
- Zuo, P., Li, Y., Liu, C.-A., Zhao, S.-H., Guan, D.-M., 2013. Coastal wetlands of China: changes from the 1970s to 2007 based on a new wetland classification system. *Estuar. Coast* 36, 390–400.